

Article

Spectral Characteristics of Nitrogen-Doped CVD Synthetic Diamonds and the Origin of Surface Blue Fluorescence

Yu Zhang , Guanghai Shi * and Zixuan Xie

School of Gemmology, China University of Geosciences (Beijing), Beijing 100083, China; zhangyu@cugb.edu.cn (Y.Z.); xzx_upup@163.com (Z.X.)

* Correspondence: shigh@cugb.edu.cn

Abstract: In recent years, many studies have been published on CVD diamond growth, but the reason for the irregular blue surface fluorescence of CVD diamond under ultra-deep UV radiation (i.e., under DiamondView) is still unclear. Here, a batch of as-grown and LPHT-annealed CVD synthetic diamond samples from a Chinese company in Zhejiang were analyzed for the various spectral (infrared (IR), UV-visible absorption, Raman, and photoluminescence (PL)) characteristics to explore the origin of surface blue fluorescence. The results show that the samples are nitrogen-doped type IIa CVD synthetic diamonds. Spectral peaks of the earlier CVD products, e.g., 3123 cm^{-1} (NVH^0) (IR absorption spectrum) and 596/597 nm (PL emission spectrum), are absent in these samples, while the peaks at 736.5/736.8 nm (SiV^-) in the UV or PL spectra are less common. PL spectra and DiamondView fluorescence indicate that the samples have generally strong luminescence peaks at 637 nm in the NV^- center, 575 nm in the NV^0 center, and other luminescence peaks caused by nitrogen-related defects. The as-grown samples observed under DiamondView show orange-red fluorescence accompanied by striations due to step-flow growth, and blue fluorescence appears as irregular threads or bundles on the surface. The LPHT-annealed sample shows weaker fluorescence with localized patches of green fluorescence contributed by weak H3 centers. The micro-IR spectra suggest that the unique blue fluorescence in the CVD diamond may be related to the dislocations caused by $\text{sp}^3\text{-CH}_2$ due to the incomplete dehydrogenation of hydrocarbon groups in the raw material.



Citation: Zhang, Y.; Shi, G.; Xie, Z. Spectral Characteristics of Nitrogen-Doped CVD Synthetic Diamonds and the Origin of Surface Blue Fluorescence. *Crystals* **2024**, *14*, 804. <https://doi.org/10.3390/cryst14090804>

Academic Editor: Yuri N. Palyanov

Received: 9 August 2024

Revised: 2 September 2024

Accepted: 10 September 2024

Published: 11 September 2024



Copyright: © 2024 by the authors. Licensee MDPI, Basel, Switzerland. This article is an open access article distributed under the terms and conditions of the Creative Commons Attribution (CC BY) license (<https://creativecommons.org/licenses/by/4.0/>).

Keywords: CVD synthetic diamond; nitrogen-doped; IR spectroscopy; PL spectra; LPHT-annealed

1. Introduction

Diamond is adored by many for its rarity, clarity, and durability. With the increasing demand for diamonds and rapid technological advancement, there is an increasing presence of synthetic (also known as cultivated) diamonds in the market, and the cost of synthetic diamond production is decreasing [1]. There are two ways to synthesize diamonds: Chemical Vapor Deposition (CVD) and High-Pressure High-Temperature (HPHT) [1,2], among which the former is important in superhard material science and gemology.

The detection of synthetic diamonds requires a profound understanding of the differences between natural and synthetic diamonds (e.g., in terms of impurities and their spatial distribution), which are resulted from their different growth environments [3]. Diamonds generally fall into two classes according to their nitrogen (N) impurity: N-bearing type I (type Ia with aggregated N impurity; type Ib with isolated N atoms) and N-free type II (type IIa with no detectable nitrogen in infrared (IR) absorption; type IIb with boron impurity) [3–5]. The CVD technique comprises the adsorption, diffusion, reaction, and desorption of carbon-bearing reactive groups and hydrogen atoms on the substrate surface (usually a small piece of a synthetic diamond as a seed crystal) by the microwave plasma method using hydrogen and methane as raw materials [1,6]. CVD synthetic diamonds are mainly type Ib and IIa. Hydrogen (the main impurity) and some other elements (e.g., N,

Si, and B) are intentionally/unintentionally introduced into the gas mixture [7–9]. Lattice defects and impurities could affect the diamond properties. A main advantage of the CVD method is the ability to dope synthesized diamonds by controlled addition of gases with the intended impurities [7]. CVD diamonds are also treated after growth, including high-temperature treatment at high pressures (HPHT) or high-temperature annealing at low pressures (LPHT) to lighten or remove brown color [7,10–12]. These treatments cause changes to defect concentrations and spectroscopic features, thereby contributing to the identification of diamonds [6,13]. CVD synthetic diamonds have good optical properties, thermal conductivity, and very high hardness and thus have a wide range of applications in both gemstone and material fields [1,14]. Manufacturers have been constantly trying new growth and post-treatment methods to improve product quality.

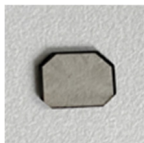
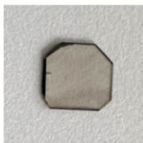
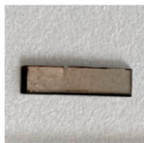
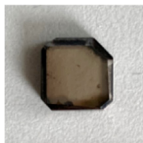
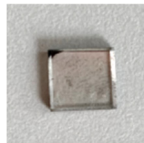
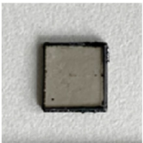
In recent years, a considerable amount of research has been dedicated to CVD diamond growth, but the reason for the irregular blue surface fluorescence of CVD diamonds under ultra-deep UV radiation (i.e., under DiamondView) is still unclear [6,11,13,15]. Here, we analyzed a batch of as-grown and LPHT-annealed CVD synthetic diamonds produced by a Chinese manufacturer in Zhejiang on their various spectral characteristics (incl. IR, UV–visible (vis) absorption, Raman, and PL emission) to explore the origin of surface blue fluorescence.

2. Materials and Analysis Methods

2.1. Materials

Six representative CVD synthetic diamond samples (CVD-1 to CVD-6) were selected from the manufacturer’s products, of which CVD-5 is an LPHT-annealed CVD synthetic diamond and the rest are as-grown CVD synthetic diamond. Their morphological features are summarized in Table 1. The CVD synthetic diamond samples are generally tabular and transparent, with adamantine luster and color ranging from colorless to light brown. The surfaces of CVD-1 and -2 were cut and polished, and the other samples were in the original growth state. The black margins of CVD-4 and CVD-6 were retained, while those of the other samples were cut off to facilitate the test of the main part. CVD synthetic diamonds are grown on a substrate (a small piece of synthetic diamond as a seed crystal) to form tablets. The tablet plane is the (100) plane of the crystal, and the growth direction is perpendicular to the substrate [1]. Meanwhile, black inclusions are present in most of the samples (e.g., CVD-3 to CVD-6).

Table 1. Summary of morphological features of the CVD synthetic diamond samples.

Sample	CVD-1	CVD-2	CVD-3	CVD-4	CVD-5	CVD-6
Image						
Color	Very light brown	Very light brown	Light brown	Brown	Colorless	Light brown
Shape	Truncated rectangular tablet	Truncated square tablet	Rectangular tablet	Truncated square tablet	Square tablet	Square tablet
Size (mm)	8.8 × 6.6 × 0.4	7.9 × 7.6 × 0.5	11.2 × 2.8 × 0.8	8.7 × 8.6 × 3.1	7.1 × 7.1 × 1.3	7.8 × 7.1 × 1.2
Weight (ct)	0.41	0.47	0.38	3.63	1.12	0.82
Internal/external features	Pure	Pure	Clear layer growth pattern on unpolished surfaces. Black flocculent inclusions.	Black flocculent and spotty inclusions in diamonds and on their margins.	Small pits and white burn marks on the surface. Black dotted inclusions.	Black flocculent and spotty inclusions.

2.2. Analysis Methods

Internal and external characteristics of the samples were observed under a GI-M2S6E gem microscope (manufacturer: Nanjing Baoguang Testing Technology Co. Ltd., Nanjing, China), while abnormal birefringence phenomena of the samples were observed under an Olympus BX51 polarizing microscope (manufacturer: Olympus Corporation, Tokyo, Japan). The fluorescence/phosphorescence properties and the growth characteristics were examined using the Diamond Trading Company's (DTC) DiamondView ultrashort-wave UV (<230 nm) luminescence imaging system (manufacturer: De Beers institute of diamonds, London, UK) [16].

The UV-Vis absorption spectra of the samples were measured with a GEM-3000 spectrophotometer at the Guangzhou Biaoqi Testing Technology Co. Ltd. (Guangzhou, China). The spectrophotometer has a 220–1000 nm analysis range, 0.5 nm resolution, 220 ms integration time, and 2 nm smoothing width.

Infrared absorption spectroscopy is useful for identifying the types of impurities and defects in diamond lattices [3]. Diamonds show important absorption features in the mid-IR range (ca. 4000–400 cm^{-1}). Our samples were analyzed by both in situ and micro-IR spectroscopy. The in situ IR spectra were measured with a Bruker TENSOR 27 Fourier transform infrared spectrometer (FTIR) (manufacturer: Bruker Corporation, Karlsruhe, Germany) at room temperature (25 °C), using the reflection method. The scanning range was set at 4000–400 cm^{-1} , with 32 scans and 4 cm^{-1} resolution. The evenly grown pure crystal portion, black margin, and black inclusion parts of samples were analyzed with a Bruker LUMOS micro FTIR spectrometer (μ FTIR) (manufacturer: Bruker Corporation, Karlsruhe, Germany) at liquid nitrogen temperature (−196.15 °C), using the transmission method. The scanning range was set at 4000–600 cm^{-1} , with 64 scans and 4 cm^{-1} resolution.

The HR-Evolution HORIBA laser Raman spectrometer (manufacturer: HORIBA Scientific, Longjumeau, France) was used to measure the Raman spectra with 532 nm excitation, two scans at 4000–100 cm^{-1} range, and 20 s integration time. The same instrument was also used to measure the PL spectra at 532 nm (540–1000 nm analysis range, two scans, 3 s integration time) and 325 nm excitation (330–800 nm analysis range, 2 scans, 3 s integration time) at liquid nitrogen temperature, respectively.

All the analyses were carried out at the Gemology Experimental Teaching Center of the China University of Geosciences (Beijing). Data processing and spectral mapping were conducted using Origin 2023 software (OriginPro 2023 10.0.0.154, Learning Version).

3. Results

3.1. Microscopic Observation

Under the gem microscope (40 \times), layered growth texture is observed on the unpolished plane of CVD-3 (Figure 1a), which is a typical growth feature of CVD synthetic diamonds. Layered growth structure was observed on the side (Figure 1d). Under the microscope, CVD-3 shows noticeable variations in the growth layer spacing in different regions (Figure 1a–c). During the CVD synthesis, the positively charged carbon ions in hydrocarbons (CH_4 , C_2H_2 , and C_6H_6) precipitate on the negatively charged substrate to form a layered growth structure parallel to the (100) plane at a rate of $\sim 6 \mu\text{m}$ per hour [1,2]. The black serrated margin of the “as-grown” tablets is often stacked by octahedrons under the microscope (Figure 1e,f). IR and Raman spectra confirmed that the black margin is a polycrystalline diamond phase. Black flocculent and spotty inclusions in CVD synthetic diamonds were observed under the gemological microscope (Figure 1g,h).

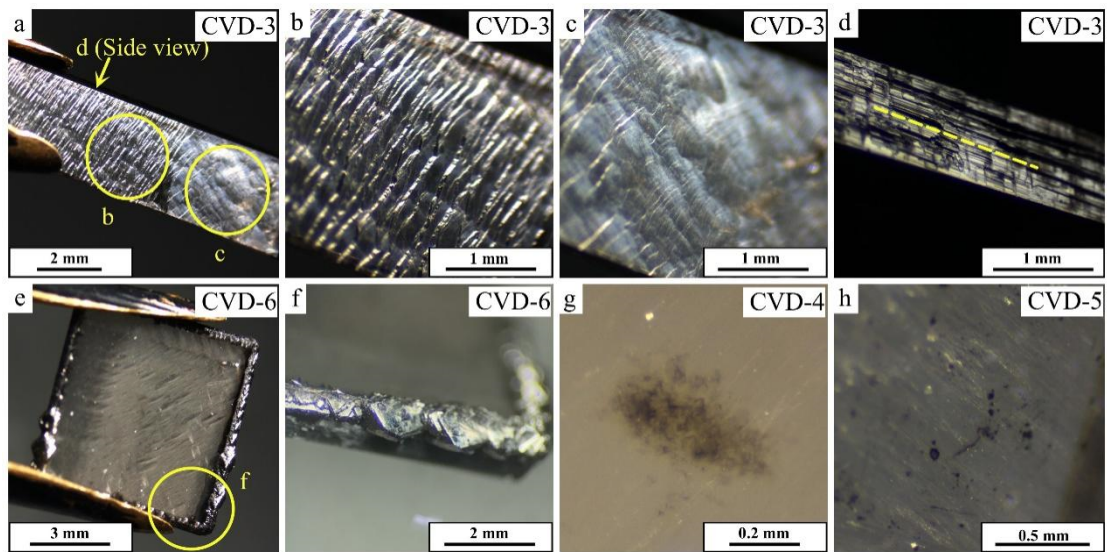


Figure 1. Microscopic photos of the CVD synthetic diamonds: (a) parallel growth texture on the unpolished sample surface; (b) zoom-in of the yellow open circle in (a), showing loose layered growth texture; (c) zoom-in of the yellow open circle in (a), showing compact layered growth texture; (d) side view of the sample with a parallel layered structure; (e) black polycrystalline margin; (f) zoom-in of the yellow open circle in (e), showing the jagged margin formed by stacked octahedrons; (g) common black fine inclusion aggregates; (h) black spotty inclusions and the white burn marks (local oxidation marks formed by overheating during the later polishing stage).

3.2. Abnormal Birefringence

Clear-banded and gridded abnormal birefringence was observed in all the samples under crossed polar (Figure 2b,c). The abnormal birefringence is more intense along the margin and around inclusions (Figure 2a,d). The strains and defects inside the CVD synthetic diamond may have caused abnormal birefringence, such as banding and gridding [17]. In contrast, the abnormal birefringence of natural diamonds is usually mottled, banded, or cross-hatched “tatami” strain [18,19]. CVD synthetics show higher-order interference colors than those generally seen in type IIa natural diamonds, though not always diagnostic [1].

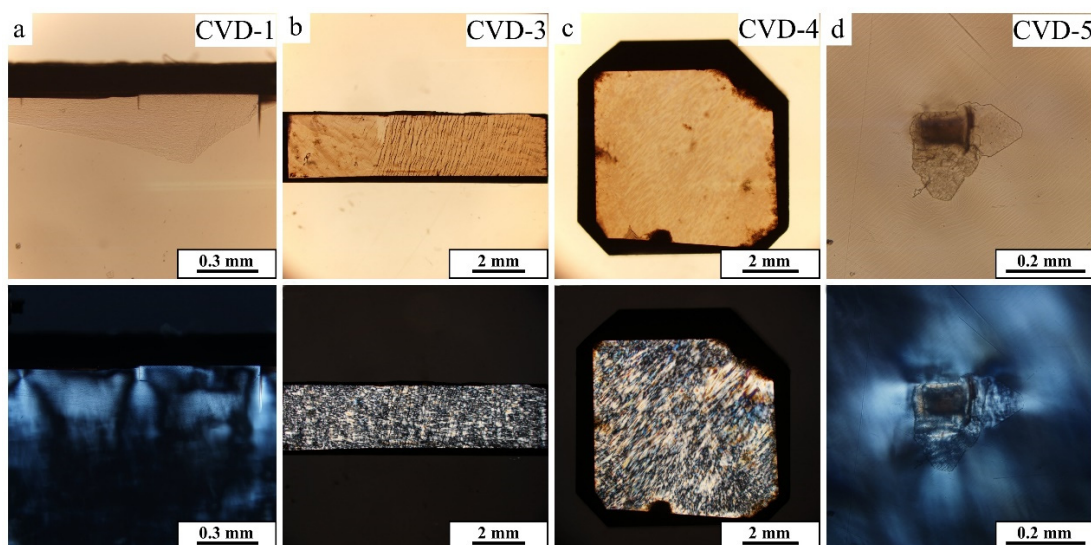


Figure 2. Samples observed under plane polarized light and crossed polarized light. Top row: plane polar; bottom row: crossed polar. (a,d) show abnormal birefringence is more intense along the margin and around inclusions; (b,c) show clear-banded and gridded abnormal birefringence.

3.3. DiamondView Examination

The DiamondView provides ultrashort-wave UV fluorescence images that can reveal distinctive fluorescence patterns of CVD synthetic diamonds. The main body of the single-crystal diamond sample shows orange-red fluorescence with striations due to step-flow growth, while the black margin and some black inclusion aggregates show blue fluorescence (Figure 3a–f). The blue fluorescence also occurs in a dendritic grid pattern or as irregular threads or bundles on the crystal surface of CVD-3 to -6 (Figure 3b–e). The fluorescence of CVD-5 was weak; dark red and green fluorescent plaques appeared locally (Figure 3d). No samples underwent a phosphorescence reaction.

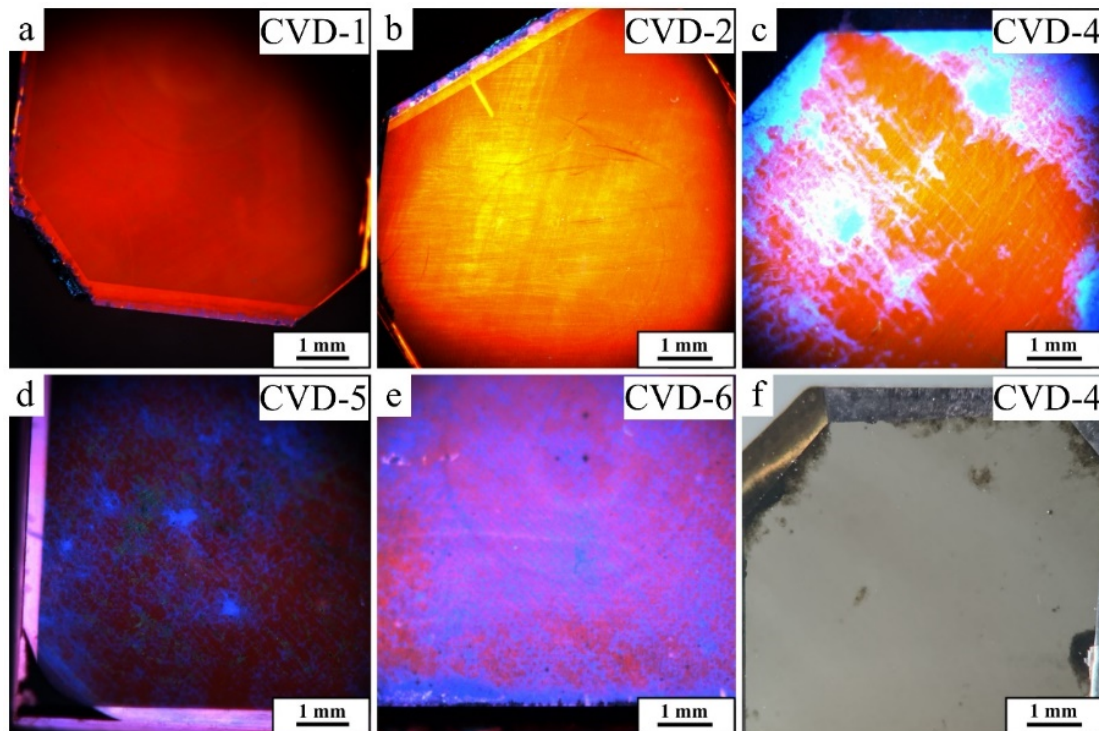


Figure 3. DiamondView images showing orange-red fluorescence (a) and striations due to the step-flow growth of CVD synthetic diamonds (b). (c,f) show the same position images of CVD-4 under ultrashort-wave UV and natural light, respectively. Irregular threads or bundles of blue fluorescence are seen, as well as a black rim and some inclusions with particularly strong blue fluorescence. (d) shows weak, dark red fluorescence, weak dendritic blue fluorescence, and yellowish-green fluorescent spots of CVD-5, and green fluorescent plaques appeared locally. (e) shows red fluorescence and gridded blue fluorescence of CVD-6.

3.4. Infrared (IR) Spectra

3.4.1. In Situ IR Spectra

The mid-IR absorption spectra of the diamond samples fall mainly in the $1500\text{--}1000\text{ cm}^{-1}$ and $3200\text{--}2800\text{ cm}^{-1}$ ranges, of which the former is more important.

In situ transmission IR spectroscopy was performed on the impurity-free regions of the samples, and the results are shown in Figure 4. The main absorption characteristics of the samples are roughly the same, with absorption peaks at 2158 , 2030 , and 1974 cm^{-1} . The absorption peaks in $1700\text{--}2700\text{ cm}^{-1}$ are intrinsic to all diamond IR spectra, which are generated by the C-C bond vibration [1].

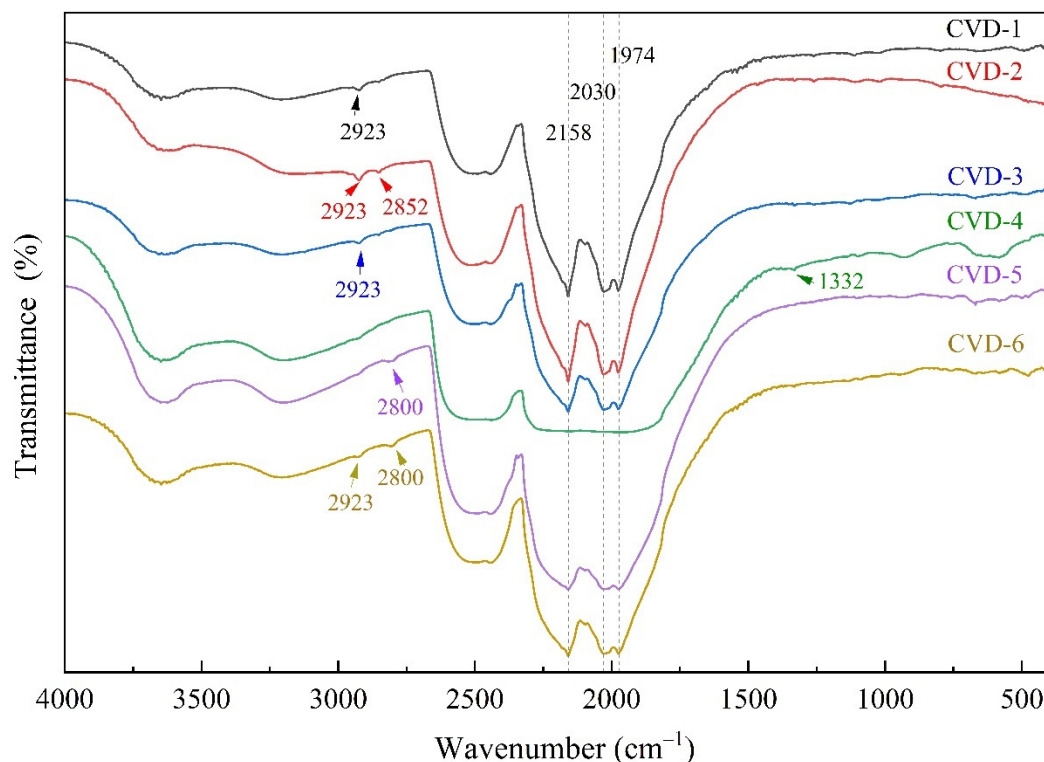


Figure 4. The in situ IR spectra of the CVD synthetic diamond samples.

Sample CVD-1, -2, and -3 have more distinct 2923 and 2853 cm^{-1} peaks, while CVD-5 and -6 have a flat and weak absorption peak at 2923 cm^{-1} and a weak peak at 2800 cm^{-1} . As for CVD-4, the 2923 and 2853 cm^{-1} peaks are largely invisible. The absorption peaks in 2800–3200 cm^{-1} denote the C-H stretching region [2,20–22]. CVD-4 also lacks absorption peaks at 2158, 2030, and 1974 cm^{-1} . It has a weak absorption peak at 1332 cm^{-1} , which is absent in other samples. In the FTIR spectrum of CVD-4, a weak absorption at 1332 cm^{-1} (caused by solitary nitrogen) is present, which is common in brown CVD diamonds [23].

There are no major nitrogen-related (e.g., 1175, 1282, 1130, and 1344 cm^{-1}) and boron-related (e.g., 2930, 2803, and 2458 cm^{-1}) absorption peaks [3], suggesting that these CVD synthetic diamonds are of type IIa.

3.4.2. Micro-Infrared Spectroscopy (μ FT-IR)

The impurity-free part of the samples and the dark margin and inclusions were analyzed, with the results illustrated in Figures 5 and 6.

The spectra of the impurity-free part of the sample are the same, with characteristic absorption peaks at 2353, 2158, 2030, and 1974 cm^{-1} , and weak 2920 (2917) and 2847 cm^{-1} absorption peaks above 2700 cm^{-1} (Figure 5). The absorption characteristics of dark inclusions and black margin in the 1750–2750 cm^{-1} range are the same as those of the impurity-free part, yet they have distinct absorption peaks at 2920 (2917), 2850 (2848), and 2818 cm^{-1} (Figure 6). Some dark impurities have absorption peaks at 1573, 1538, 1455, and 875 cm^{-1} , and the attribution of these peaks is not clear (Figure 6).

Vibrational modes at 3123 cm^{-1} (NVH^0) [24] and 3107 cm^{-1} (N_3VH^0) [25] were not detected in any of the samples.

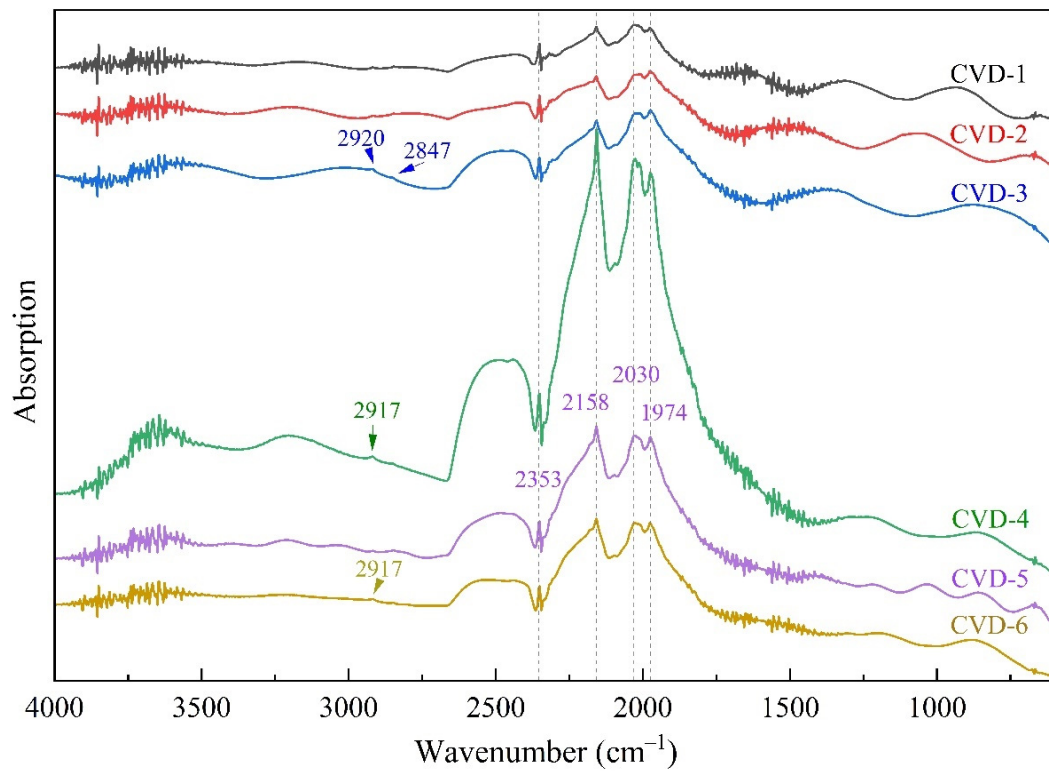


Figure 5. Micro-IR spectra of the impurity-free part of the CVD synthetic diamond samples.

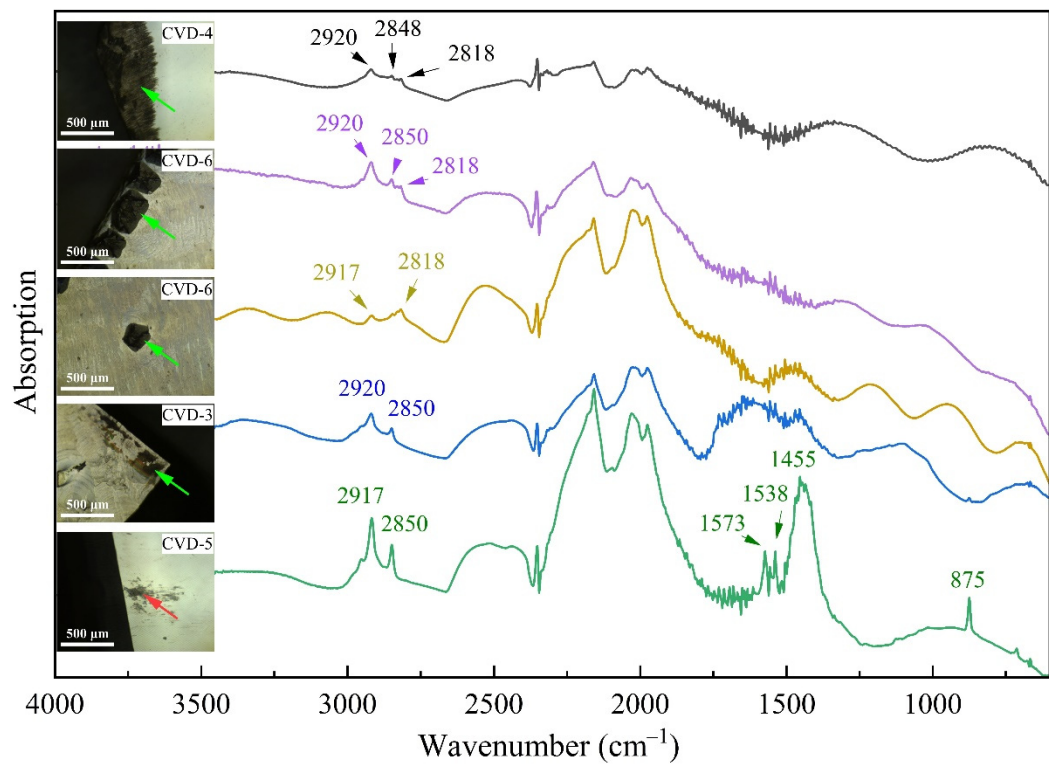


Figure 6. Micro-IR spectra of the dark inclusions and margins of the CVD synthetic diamond samples.

3.5. UV–Vis Absorption Spectra

The UV–Vis absorption spectra of the samples are shown in Figure 7. A broad absorption band centered at ~ 270 nm is present in all the as-grown samples (CVD-1 to -4 and -6), accompanied by an absorption step at 360 nm. The 270 nm band is weak in CVD-5 (LPHT-annealed samples), while the broad 360 nm band is largely invisible. The very weak 595 nm peaks are present in CVD-3, -4, and -6. The absorption peak at 737 nm was only detected in CVD-4.

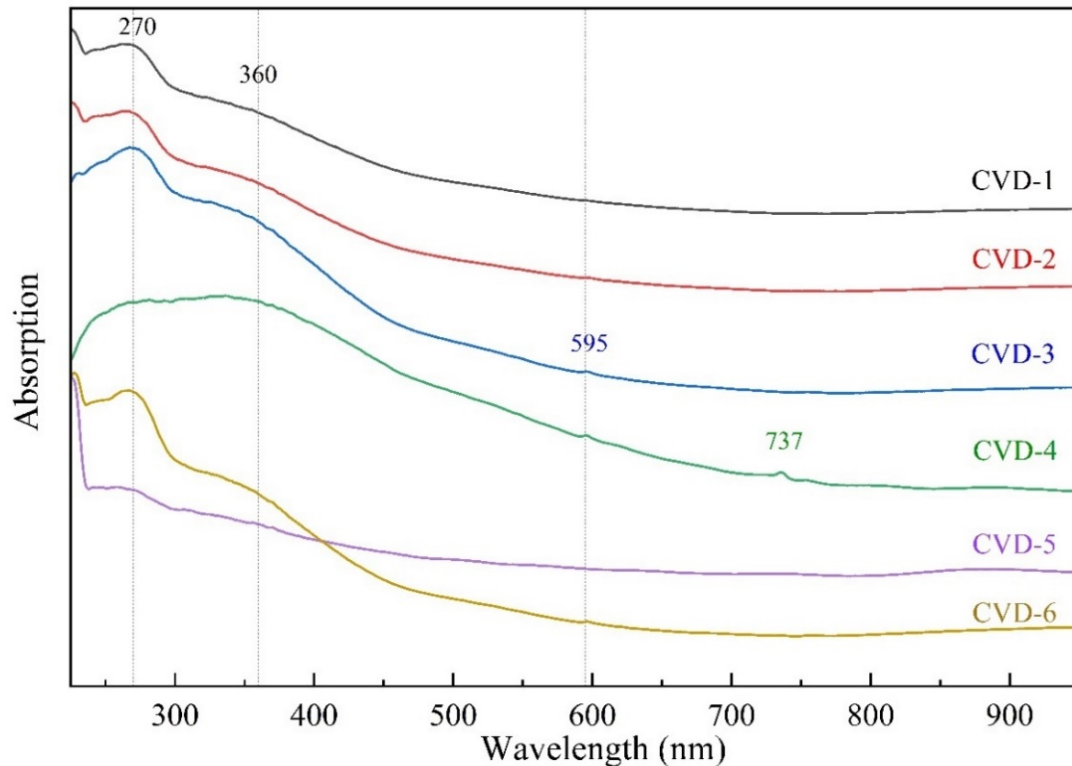


Figure 7. UV–Vis absorption spectra of the CVD synthetic diamond samples.

3.6. Raman Spectroscopy

Raman spectra were measured on the impurity-free parts of the samples, and the results are shown in Figure 8. All samples have a diamond intrinsic peak at 1332 cm^{-1} . The narrow full width at half maximum (FWHM) of peaks reflects the good crystallinity of these samples. Except for CVD-5, the other samples have characteristic peaks at 1416 cm^{-1} , with that in CVD-6 being the most prominent. This peak is not the intrinsic Raman spectra of the material. It is unrelated to the carbon of the non-diamond phase but is a fluorescence peak generated by the excitation of the NV^0 center. The generation of this fluorescence peak can be avoided by increasing or decreasing the excitation wavelength of the analysis [26]. The 1590 cm^{-1} peak in CVD-5 may be an offset of the G-band (graphitic peak) [26–28].

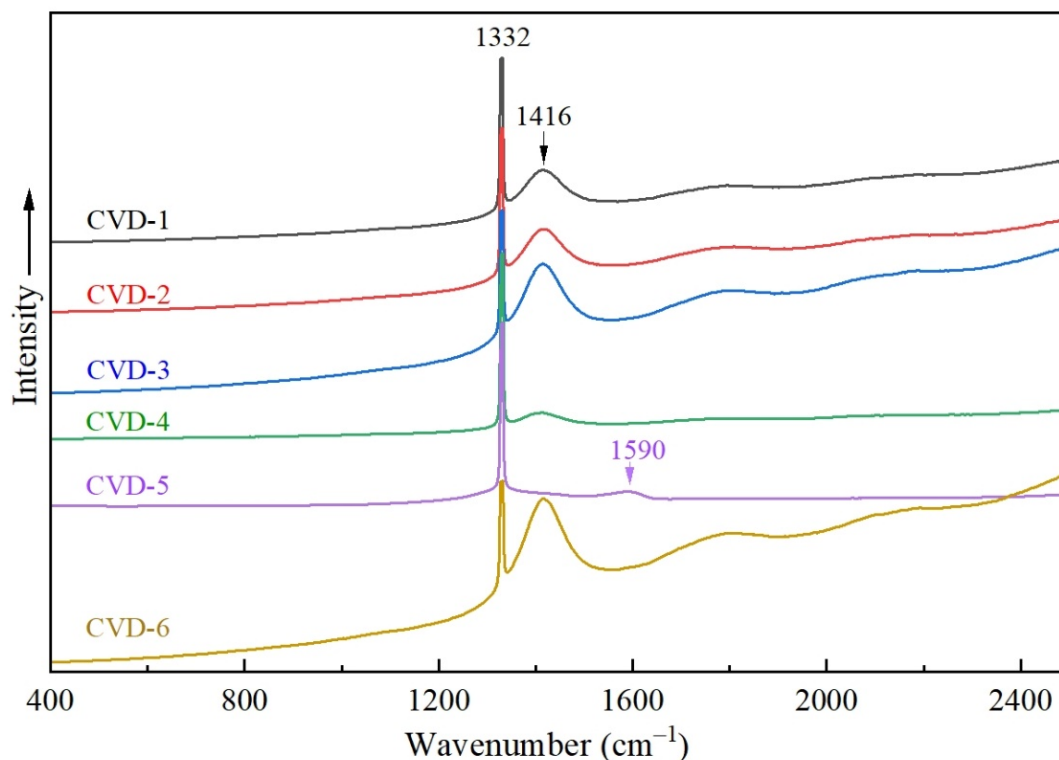


Figure 8. Raman spectra of the CVD synthetic diamond samples.

3.7. Photoluminescence (PL) Spectroscopy

PL spectroscopy is highly sensitive and can detect optical defects at much lower concentrations than absorption spectroscopy. Therefore, the PL spectral (spectral features excited by incident laser) can detect the optical centers in diamonds when Vis-NIR absorption cannot [1]. The PL spectra of all the impurity-free regions of the samples were measured with two laser excitations of 532 nm (Figures 9 and 10) and 325 nm (Figure 11) under liquid nitrogen temperature.

With the 532 nm laser excitation, all six samples have significant characteristic emissions at 573, 575, and 637 nm. 573 nm is the intrinsic diamond-related Raman peak [29]. Except for CVD-4, the ZPL of the other samples at 637 nm is stronger than that at 575 nm. Only CVD-4 has a significant 736.5/736.8 nm doublet associated with the SiV^- center, accompanied by a very weak and broad peak at 766 nm. In contrast, 736.5/736.8 nm doublet is completely absent in CVD-1, -2, and -3, and very weak in CVD-5 and -6.

The most significant PL spectra with the 325 nm laser excitation are the peaks at 575 nm (present in all the samples) and 736.5/736.8 nm doublet (only in CVD-4 and CVD-6). A weak 503.2 nm peak appeared in the LPHT-annealed sample (CVD-5).

The 596/597 nm doublet, which was previously considered to be a common feature of (near-)colorless to brown as-grown CVD synthetics [10,11,30], is absent in all of our samples.

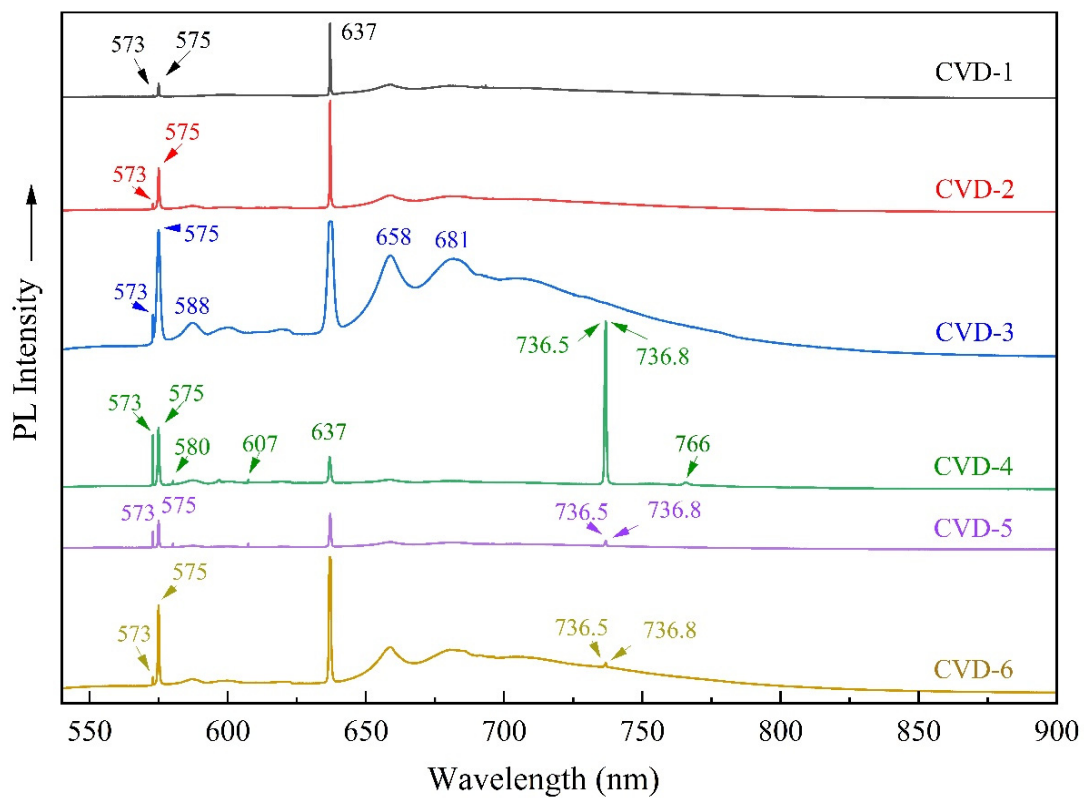


Figure 9. PL spectra of the samples measured with 532 nm laser excitation.

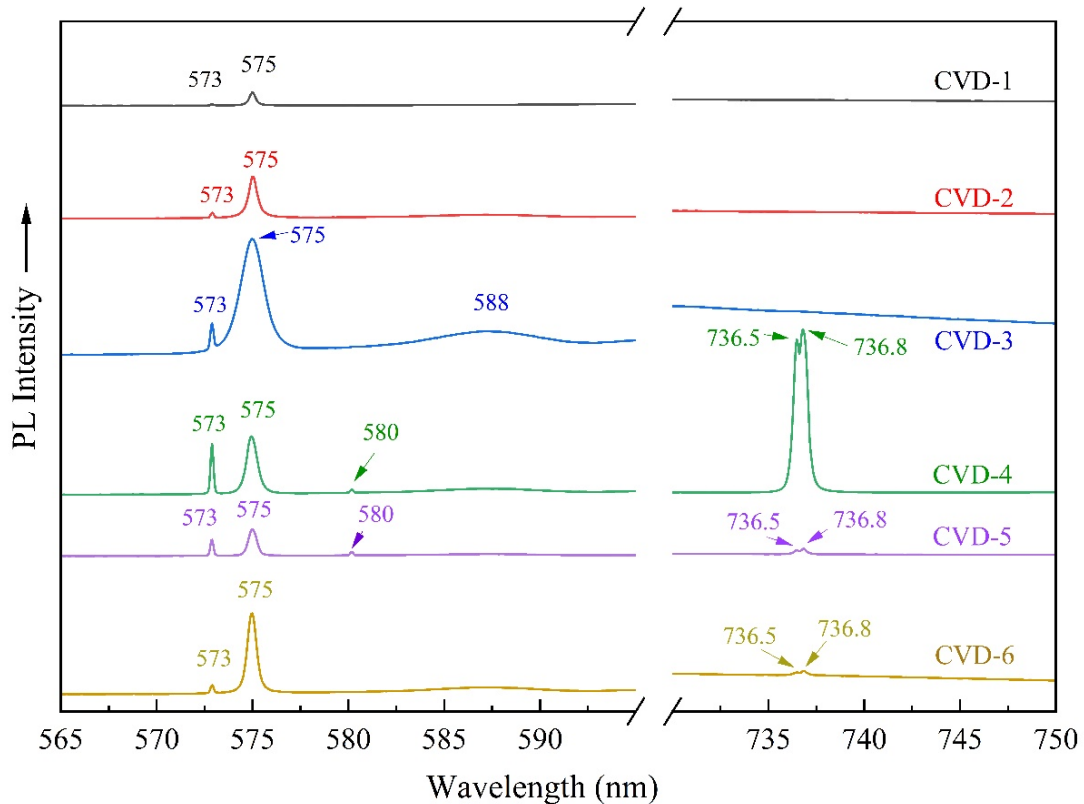


Figure 10. The 575 nm and 736.5/736.8 nm doublet in PL spectra (measured with 532 nm laser excitation).

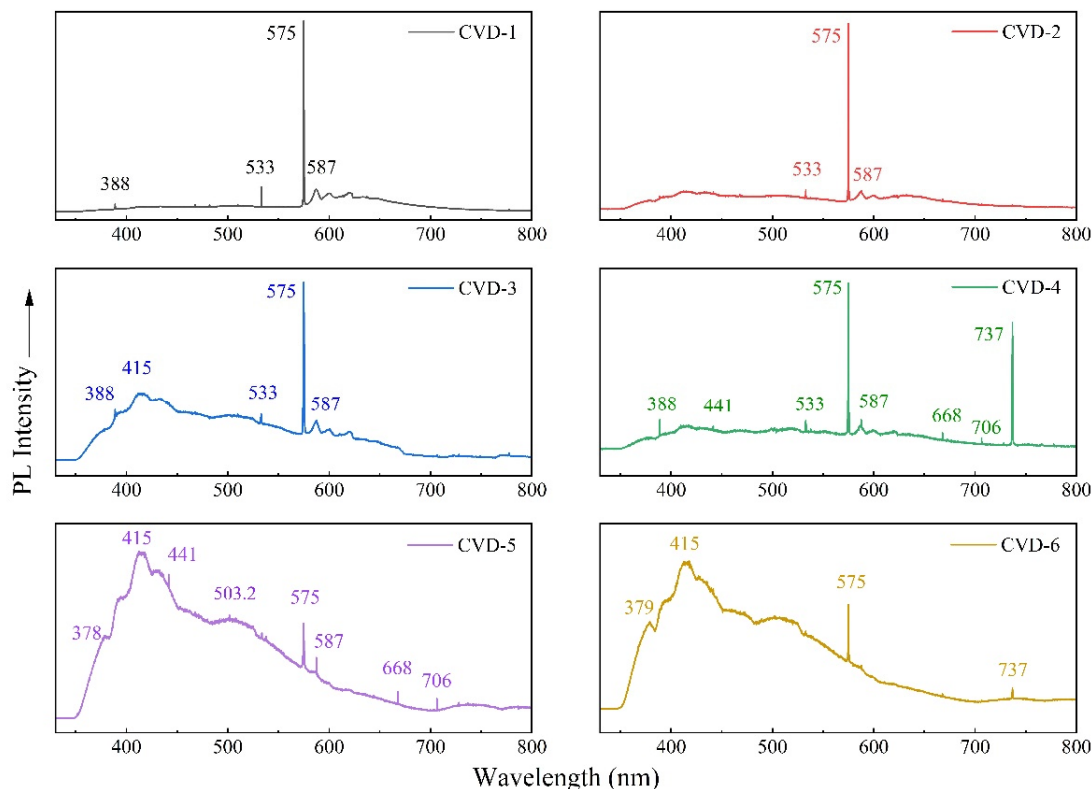


Figure 11. PL spectra of the samples measured with 325 nm laser excitation.

4. Discussion

4.1. Nitrogen Defects in CVD Synthetic Diamonds

In the PL spectra, the as-grown samples generally have luminescence peaks caused by nitrogen-related defects, such as the 637 nm peak, which is attributed to the negatively charged N-vacancy optical defects NV^- [31] and the 575 nm peak of the NV^0 center [32,33], but lack the H3 (NVN^0) center (with ZPL at 503.2 nm) caused by a defect with two nitrogen atoms adjacent to a single vacancy (Figure 9) [34,35]. The broad UV-Vis absorption band at ~ 270 nm and absorption step at 360 nm are likely caused by isolated ppm-level nitrogen [5,30]. Based on this absorption peak, it is implied that the diamond is CVD synthetic, HPHT synthetic (Ib-type), or HPHT-treated natural diamond (type-II) [36]. The luminescence under DiamondView varies with the type of defects in the diamond. Most unprocessed CVD synthetic diamonds have usually orange-red/-yellow fluorescence due to the dominance of NV defects [1,37]. Meanwhile, there is no discernible 1344 cm^{-1} absorption peak in the IR spectra. This indicates that the samples are type IIa with trace nitrogen, consistent with the orange-red fluorescence under DiamondView.

Pure CVD synthetic diamonds are nitrogen-free type IIa. The growth rate of CVD diamonds can be significantly increased by doping trace amounts of nitrogen [38]. Type IIa CVD synthetic diamonds (no discernible absorption at 1344 cm^{-1}) can be grown even when doped with nitrogen [11]. Nitrogen-doped CVD synthetic diamonds are usually brown and less appealing than other colors due to the introduction of nitrogen vacancies and hydrogen complexes [11]. Post-synthetic treatments (e.g., HPHT and/or irradiation and annealing) are applied to lighten the color or to create attractive colors (e.g., pink) [39].

4.2. Silicon Vacancy

Compared with known CVD diamond products, the probability of silicon vacancies in this manufacturer's products is lower. Only CVD-4 (as-grown) has a significant 736.5/736.8 nm doublet associated with the SiV^- center, accompanied by a very weak and

broad peak at 766 nm. In contrast, the 736.5/736.8 nm doublet is completely absent in CVD-1, -2, and -3 (these three are as-grown samples) and very weak in CVD-5 (LPHT-annealed) and -6 (as-grown) (Figures 9 and 10).

The 736.5/736.8 nm doublet in the PL spectrum is related to the SiV^- vibration, which is formed by the negative charge of silicon impurities and vacancy that are common in CVD synthetic diamonds [1,7,11,30,40,41]. The SiV^- center is frequently observed in the UV–Vis absorption spectra with the 737 nm peak (Figure 7, e.g., CVD-4) [11,30,40]. Since Si-containing materials are usually used as cavities and substrates in CVD synthetic diamond equipment, Si atoms in the environment would inevitably enter the CVD synthetic diamond lattice under chemical vapor deposition growth conditions. As a result, Si defects are common in CVD synthetic diamonds. In contrast, Si defects are rarely present in HPHT synthetic diamonds, unless Si is artificially doped in the catalyst or denitrifying agent [42,43]. The SiV^- center is also visible in very few natural diamonds, but is generally weak [41].

The 736.5/736.8 nm doublet or the 737 nm peak caused by the vibration of SiV^- was once considered diagnostic for CVD synthetic diamonds. However, we found that many CVD products lack this spectral feature. Previous studies have shown that the PL intensity at 737 nm greatly weakens after HPHT or LPHT annealing [12]. Therefore, it is necessary to consider other features to determine whether the diamond is CVD synthetic.

4.3. Comparison of Spectral Characteristics of As-Grown and LPHT-Annealed Samples

All samples show similar infrared spectra. LPHT annealing did not cause significant changes in the infrared absorption spectrum. It is noteworthy that 3123 cm^{-1} IR absorption peaks are absent in all our samples. The 3123 cm^{-1} (NVH^0) band is caused by the neutral charge state of the nitrogen vacancy–hydrogen complex [2,24], which is common in nitrogen-doped CVD synthetic materials [10,11,24,44,45]. The 3123 cm^{-1} absorption band disappears after HPHT treatment but may still be present in LPHT-annealed CVD diamonds [12]. The absence of 3123 cm^{-1} could also be due to the growth of transparent CVD diamonds without nitrogen addition. However, in this study, both the N-doped as-grown samples and the LPHT-annealed sample show the absence of 3123 cm^{-1} .

Raman spectroscopy is highly sensitive for detecting amorphous carbon and graphite. No distinct D-band (disorder band, near 1350 cm^{-1}) associated with microcrystalline graphite or amorphous carbon was detected in our samples [26,27]. The 1590 cm^{-1} peak in CVD-5 may be an offset of the G-band (graphitic peak) [26–28], which is possibly caused by the local graphitization via LPHT annealing. The LPHT annealing lightens the color (CVD-5), increases the transmittance, and weakens the UV–Vis absorption at 270 and 360 nm.

The difference in PL spectra between the as-grown and LPHT-annealed samples is very weak. A weak 503.2 nm emission peak appeared in the LPHT-annealed sample (CVD-5) under only 325 nm excitation. Previous studies have shown that after LPHT annealing, the relative intensity of negatively charged optical centers (such as NV^- , with ZPL at 637 nm) decreases, while the relative intensity of neutrally charged centers (such as NV^0 and H3 (NVN^0), with ZPL at 575 nm and 503.2 nm, respectively) increases [12]. In this study, the NV^- and NV^0 centers of the LPHT annealing samples did not change regularly compared to those of the as-grown samples, but the LPHT annealing samples showed weak H3 centers. During the LPHT annealing process, some isolated nitrogen atoms in the diamonds form aggregates and then capture the vacancy to form H3 (NVN^0) centers locally. This reduces the NV centers and lightens the color of the diamonds, weakening the red fluorescence and giving rise to yellow-green fluorescent speckles under DiamondView [2,3,35,37].

4.4. Unique Fluorescence under DiamondView

CVD synthetic diamonds have a variety of fluorescence reactions when exposed to ultra-deep UV radiation due to defects in the diamond lattice [13]. The dominant orange-

red fluorescence is usually observed in N-doped CVD synthetic diamond and is due to the NV centers [1]. The orange fluorescence with irregular blue fluorescence patterns under DiamondView is unique to N-doped CVD synthetic diamonds [30]. Figure 3c shows that the irregular blue fluorescence in the sample is stronger at the black edge of the sample and the dark inclusions. Previous studies showed that the irregular blue fluorescence originates from the band-A emission, which is caused by structural dislocations [11,46]. Dislocations are extended defects in the diamond structure and often originate from the interface between the CVD synthetic diamond substrate and the growth layer [11,47].

In situ IR spectra showed that the samples showed absorption peaks near 2920 and 2850 cm^{-1} in the C-H stretching region, which is associated with the $\text{sp}^3\text{-CH}_2$ vibration [2,20–22,48]. Micro-IR spectra showed that compared with the evenly grown pure crystal portion, the dark margin and inclusions (Raman and micro-infrared spectra identified as part of the diamond phase) show more distinct absorption peaks at 2920 and 2850 cm^{-1} and thus have more abundant $\text{sp}^3\text{-CH}_2$ structures. The blue fluorescence of the black margin and inclusions is significantly stronger than that of the pure crystal portion under DiamondView. Considering also that the content of $\text{sp}^3\text{-CH}_2$ has a positive correlation with the intensity of the irregular blue fluorescence, it is inferred that the irregular blue fluorescence may be related to $\text{sp}^3\text{-CH}_2$ structures.

The surfaces of CVD-1 and CVD-2 were cut and polished, which greatly reduced the blue fluorescence (see Figure 3a,b), suggesting that this blue fluorescence is often enriched near the boundaries of the crystals. Previous studies showed that the band-A emission appeared only at nonepitaxial crystallite sites, not observed in the high-quality crystal of CVD synthetic diamonds without nonepitaxial crystallites [46]. The nonepitaxial crystallites contained defects such as dislocations and several types of grain boundaries [46].

These $\text{sp}^3\text{-CH}_2$ structure absorption spectra and blue fluorescence only appear in CVD synthetic diamonds, which is possibly due to the incomplete dehydrogenation of hydrocarbon groups in the raw material (such as CH_4) during the CVD diamond growth process. Crystallization is unstable at the very beginning or near the end of CVD diamond growth, and more $\text{sp}^3\text{-CH}_2$ structures appeared at nonepitaxial crystallite sites (close to the boundary) to form dislocations producing irregular blue fluorescence. Step-flow growth of CVD synthetic diamonds may cause the dislocations to deviate, following a zigzag path [15]. Finally, we observed blue fluorescence in CVD diamonds in the form of irregular threads or bundles, which may be patchy.

5. Conclusions

IR, Raman, PL, and UV–Vis spectroscopy show that the CVD synthetic diamond samples are nitrogen-doped IIa-type with high crystallinity. Compared to the as-grown samples, the LPHT annealing sample (CVD-5) shows a weak 503.2 nm peak in the PL spectra. The LPHT annealing treatment lightens the color, increases the transmittance, weakens the UV–Vis absorption at 270 and 360 nm, and weakens the red fluorescence under DiamondView and forms yellowish-green fluorescent speckles, while the local graphitization forms the broad 1590 nm Raman spectral peak.

The intensities of the 2920 and 2850 cm^{-1} absorption peaks in the micro-IR spectra show a positive correlation with the intensity of the irregular blue fluorescence under DiamondView, which indicates that the blue fluorescence may be related to abundant $\text{sp}^3\text{-CH}_2$ structures. Incomplete dehydrogenation of hydrocarbon groups in the raw material during the unstable growth of CVD diamonds forms $\text{sp}^3\text{-CH}_2$ structures, resulting in dislocations that give rise to irregular blue fluorescence.

Specific peaks of the early CVD products, such as the 3123 cm^{-1} peak (IR spectrum) and 596/597 nm doublet (PL spectrum), are absent in our samples, while the 736.5/736.8 nm doublet is weak. A combination of the orange-red fluorescence accompanied by striations (under DiamondView), the UV–Vis absorption spectrum (broad absorption band centered at 270 nm and absorption step at 360 nm), as well as the PL (luminescence peaks at 637

and 575 nm) spectra are needed to reliably identify CVD synthetic diamonds from this manufacturer.

Author Contributions: Conceptualization, Y.Z. and G.S.; methodology, Y.Z.; software, Y.Z.; validation, Y.Z. and Z.X.; formal analysis, Y.Z.; investigation, Y.Z. and Z.X.; resources, Y.Z. and G.S.; data curation, Y.Z. and Z.X.; writing—original draft preparation, Y.Z.; writing—review and editing, Y.Z. and G.S.; visualization, Y.Z.; supervision, G.S.; project administration, G.S.; funding acquisition, G.S. All authors have read and agreed to the published version of the manuscript.

Funding: This research was funded by the National Natural Science Foundation Of China, grant number 42273044.

Data Availability Statement: The data presented in this study are available within the article.

Acknowledgments: The authors would like to thank Huzhou Sino-C Semiconductor Technology Co. Ltd. for technical support and for providing the CVD diamond samples. The authors would like to thank Yuan Y. for their laboratory technical support (School of Gemology, China University of Geosciences, Beijing).

Conflicts of Interest: The authors declare no conflicts of interest.

References

1. Eaton-Magaña, S.; Shigley, J.E. Observations on CVD-grown synthetic diamonds: A review. *Gems Gemol.* **2016**, *52*, 222–245. [[CrossRef](#)]
2. Ashfold, M.N.R.; Goss, J.P.; Green, B.L.; May, P.W.; Newton, M.E.; Peaker, C.V. Nitrogen in diamond. *Chem. Rev.* **2020**, *120*, 5745–5794. [[CrossRef](#)] [[PubMed](#)]
3. Breeding, C.M.; Shigley, J.E. The “type” classification system of diamonds and its importance in gemology. *Gems Gemol.* **2009**, *45*, 96–111. [[CrossRef](#)]
4. Fisher, D.; Evans, D.J.F.; Glover, C.; Kelly, C.J.; Sheehy, M.J.; Summerton, G.C. The vacancy as a probe of the strain in type IIa diamonds. *Diam. Relat. Mater.* **2006**, *15*, 1636–1642. [[CrossRef](#)]
5. Bogert, C.H.V.D.; Smith, C.P.; Hainschwang, T.; McClure, S.F. Gray-to-blue-to-violet hydrogen-rich diamonds from the Argyle mine, Australia. *Gems Gemol.* **2009**, *45*, 20–37. [[CrossRef](#)]
6. D’Haenens-Johansson, U.F.S.; Butler, J.E.; Katrusha, A.N. Synthesis of diamonds and their identification. *Rev. Miner. Geochem.* **2022**, *88*, 689–753. [[CrossRef](#)]
7. Wang, W.; D’Haenens-Johansson, U.F.S.; Johnson, P.; Moe, K.S.; Emerson, E. CVD synthetic diamonds from Gemesis Corp. *Gems Gemol.* **2012**, *48*, 80–97. [[CrossRef](#)]
8. Othman, M.Z.; May, P.W.; Fox, N.A.; Heard, P.J. Incorporation of lithium and nitrogen into CVD diamond thin films. *Diam. Relat. Mater.* **2014**, *44*, 1–7. [[CrossRef](#)]
9. Prieske, M.; Vollertsen, F. In situ incorporation of silicon into a CVD diamond layer deposited under atmospheric conditions. *Diam. Relat. Mater.* **2016**, *65*, 47–52. [[CrossRef](#)]
10. Wang, W.Y.; Moses, T.; Linares, R.C.; Shigley, J.E.; Hall, M.; Butler, J.E. Gem-quality synthetic diamonds grown by a chemical vapor deposition (CVD) method. *Gems Gemol.* **2003**, *39*, 268–283. [[CrossRef](#)]
11. Martineau, P.M.; Lawson, S.C.; Taylor, A.J.; Quinn, S.J.; Evans, D.J.F.; Crowder, M.J. Identification of synthetic diamond grown using chemical vapor deposition (CVD). *Gems Gemol.* **2004**, *40*, 2–25. [[CrossRef](#)]
12. Meng, Y.F.; Yan, C.S.; Lai, J.; Krasnicki, S.; Shu, H.; Yu, T.; Liang, Q.; Mao, H.K.; Hemley, R.J. Enhanced optical properties of chemical vapor deposited single crystal diamond by low-pressure/high-temperature annealing. *Proc. Natl. Acad. Sci. USA* **2008**, *105*, 17620–17625. [[CrossRef](#)]
13. Hardman, M.F.; Eaton-Magaña, S.C.; Breeding, C.M.; Ardon, T.; D’Haenens-Johansson, U.F.S. Evaluating the defects in CVD diamonds: A statistical approach to spectroscopy. *Diam. Relat. Mater.* **2022**, *130*, 109508. [[CrossRef](#)]
14. Butler, J.E.; Mankelevich, Y.A.; Cheesman, A.; Ma, J.; Ashfold, M.N.R. Understanding the chemical vapor deposition of diamond: Recent progress. *J. Phys. Condens. Matter* **2009**, *21*, 364201. [[CrossRef](#)]
15. Martineau, P.; Gaukroger, M.; Khan, R.; Evans, D. Effect of steps on dislocations in CVD diamond grown on {001} substrates. *Phys. Status Solidi (C)* **2009**, *6*, 1953–1957. [[CrossRef](#)]
16. Welbourn, C.M.; Cooper, M.; Spear, P.M. De Beers natural versus synthetic diamond verification instruments. *Gems Gemol.* **1996**, *32*, 156–169. [[CrossRef](#)]
17. Pinto, H.; Jones, R. Theory of the birefringence due to dislocations in single crystal CVD diamond. *J. Phys. Condens. Matter* **2009**, *21*, 364220. [[CrossRef](#)]

18. Smith, C.P.; Bosshart, G.; Ponahlo, J.; Hammer, V.M.F.; Klapper, H.; Schmetzer, K. GE POL diamonds: Before and after. *Gems Gemol.* **2000**, *36*, 192–215. [[CrossRef](#)]
19. Howell, D. Strain-induced birefringence in natural diamond: A review. *Eur. J. Miner.* **2012**, *24*, 575–585. [[CrossRef](#)]
20. Dischler, B.; Wild, C.; Müller-Sebert, W.; Koidl, P. Hydrogen in polycrystalline diamond. *Phys. B Condens. Matter* **1993**, *185*, 217–221. [[CrossRef](#)]
21. Titus, E.; Misra, D.S.; Sikder, A.K.; Tyagi, P.K.; Singh, M.K.; Misra, A.; Ali, N.; Cabral, G.; Neto, V.F.; Gracio, J. Quantitative analysis of hydrogen in chemical vapor deposited diamond films. *Diam. Relat. Mater.* **2005**, *14*, 476–481. [[CrossRef](#)]
22. John, P.; Milne, D.K.; Drummond, I.C.; Jubber, M.G.; Savage, J.A. IR attenuated total reflectance studies of d.c. biased growth of diamond films. *Diam. Relat. Mater.* **1994**, *3*, 486–491. [[CrossRef](#)]
23. Zaitsev, A.M.; Wang, W.; Moe, K.S.; Johnson, P. Spectroscopic studies of yellow nitrogen-doped CVD diamonds. *Diam. Relat. Mater.* **2016**, *68*, 51–61. [[CrossRef](#)]
24. Khan, R.U.A.; Martineau, P.M.; Cann, B.L.; Newton, M.E.; Twitchen, D.J. Charge transfer effects, thermo and photochromism in single crystal CVD synthetic diamond. *J. Phys. Condens. Matter* **2009**, *21*, 364214. [[CrossRef](#)] [[PubMed](#)]
25. Goss, J.P.; Briddon, P.R.; Hill, V.; Jones, R.; Rayson, M.J. Identification of the structure of the 3107 cm⁻¹H-related defect in diamond. *J. Phys. Condens. Matter* **2014**, *26*, 145801. [[CrossRef](#)] [[PubMed](#)]
26. Zhu, R.H.; Liu, J.L.; Chen, L.X.; Wei, J.J.; Li, C.M. Research on 1420 cm⁻¹ characteristic peak of free-standing diamond films in Raman spectrum. *Rengong Jingti Xuebao/J. Synth. Cryst.* **2015**, *44*, 867–871, (In Chinese with English Abstract).
27. Ismagilov, R.; Malykhin, S.; Puzyr, A.; Loginov, A.; Kleshch, V.; Obratsov, A. Single-crystal diamond needle fabrication using hot-filament chemical vapor deposition. *Materials* **2021**, *14*, 2320. [[CrossRef](#)]
28. Pandey, M.; D’Cunha, R.; Tyagi, A.K. Defects in CVD diamond: Raman and XRD studies. *J. Alloys Compd.* **2002**, *333*, 260–265. [[CrossRef](#)]
29. Song, Z.; Lu, T.; Dai, H.; Ke, J.; Zhang, J.; Liu, H.; Zhu, W. Identification of type IIa blue CVD synthetic diamonds from Huzhou Sinoc Semiconductor Co., in China. *J. Gemmol.* **2020**, *37*, 306–313. [[CrossRef](#)]
30. Wang, W.Y.; Hall, M.S.; Moe, K.S.; Tower, J.; Moses, T.M. Latest-generation CVD-grown synthetic diamonds from Apollo Diamond Inc. *Gems Gemol.* **2007**, *43*, 294–312. [[CrossRef](#)]
31. Zaitsev, A.M.; Moe, K.S.; Wang, W. Optical centers and their depth distribution in electron irradiated CVD diamond. *Diam. Relat. Mater.* **2017**, *71*, 38–52. [[CrossRef](#)]
32. Mita, Y. Change of absorption spectra in type-Ib diamond with heavy neutron irradiation. *Phys. Rev. B* **1996**, *53*, 11360–11364. [[CrossRef](#)] [[PubMed](#)]
33. Ji, P.; Balili, R.; Beaumariage, J.; Mukherjee, S.; Snoko, D.; Dutt, M.V.G. Multiple-photon excitation of nitrogen vacancy centers in diamond. *Phys. Rev. B* **2018**, *97*, 134112. [[CrossRef](#)]
34. Collins, A.T.; Connor, A.; Ly, C.H.; Shareef, A.; Spear, P.M. High-temperature annealing of optical centers in type-I diamond. *J. Appl. Phys.* **2005**, *97*, 083517. [[CrossRef](#)]
35. Fisher, D. Brown diamonds and high pressure high temperature treatment. *Lithos* **2009**, *112*, 619–624. [[CrossRef](#)]
36. Iakoubovskii, K.; Collins, A.T. Alignment of Ni- and Co-related centres during the growth of high-pressure-high-temperature diamond. *J. Phys. Condens. Matter* **2004**, *16*, 6897–6906. [[CrossRef](#)]
37. Eaton-Magana, S.; Shigley, J.E.; Breeding, C.M. Observations on HPHT-Grown Synthetic Diamonds: A Review. *Gems Gemol.* **2017**, *53*, 262–284. [[CrossRef](#)]
38. Tallaire, A.; Achard, J.; Silva, F.; Sussmann, R.S.; Gicquel, A. Homoepitaxial deposition of high-quality thick diamond films: Effect of growth parameters. *Diam. Relat. Mater.* **2005**, *14*, 249–254. [[CrossRef](#)]
39. Sheppard, R.; D’Haenens-Johansson, U.; Moe, K.S.; Moses, T.; Wang, W.Y. HPHT synthetic diamond melee in high-quality jewelry piece. *Gems Gemol.* **2015**, *51*, 64–65.
40. Wang, W.Y.; Tallaire, A.; Hall, M.S.; Moses, T.M.; Achard, J.; Sussmann, R.S.; Gicquel, A. Experimental CVD synthetic diamonds from LIMHP-CNRS, France. *Gems Gemol.* **2005**, *41*, 234–244. [[CrossRef](#)]
41. Breeding, C.M.; Wang, W. Occurrence of the Si–V defect center in natural colorless gem diamonds. *Diam. Relat. Mater.* **2008**, *17*, 1335–1344. [[CrossRef](#)]
42. D’Haenens-Johansson, U.F.S.; Katrusha, A.; Moe, K.S.; Johnson, P.; Wang, W.Y. Large colorless HPHT-grown synthetic gem diamonds from new diamond technology, Russia. *Gems Gemol.* **2015**, *51*, 260–279. [[CrossRef](#)]
43. D’Haenens-Johansson, U.F.S.; Moe, K.S.; Johnson, P.; Wong, S.Y.; Lu, R.; Wang, W.Y. Near-colorless HPHT synthetic diamonds from AOTC Group. *Gems Gemol.* **2014**, *50*, 30–45. [[CrossRef](#)]
44. Fuchs, F.; Wild, C.; Schwarz, K.; Muller-Sebert, W.; Koidl, P. Hydrogen induced vibrational and electronic transitions in chemical vapor deposited diamond, identified by isotopic substitution. *Appl. Phys. Lett.* **1995**, *66*, 177–179. [[CrossRef](#)]
45. Liggins, S. *Identification of Point Defects in Treated Single Crystal Diamond*; Department of Physics, University of Warwick: Coventry, UK, 2010.
46. Takeuchi, D.; Watanabe, H.; Yamanaka, S.; Okushi, H.; Sawada, H.; Ichinose, H.; Sekiguchi, T.; Kajimura, K. Origin of band-Aemission in diamond thin films. *Phys. Rev. B* **2001**, *63*, 245328. [[CrossRef](#)]

47. Ichikawa, K.; Shimaoka, T.; Kato, Y.; Koizumi, S.; Teraji, T. Dislocations in chemical vapor deposition diamond layer detected by confocal Raman imaging. *J. Appl. Phys.* **2020**, *128*, 155302. [[CrossRef](#)]
48. Sellschop, J.; Connell, S.; Madiba, C.; Sideras-Haddad, E.; Stemmet, M.; Bharuth-Ram, K.; Appel, H.; Kundig, W.; Patterson, B.; Holzschuh, E. Hydrogen in and on natural and synthetic diamond. *Nucl. Instrum. Methods B* **1992**, *68*, 133–140. [[CrossRef](#)]

Disclaimer/Publisher’s Note: The statements, opinions and data contained in all publications are solely those of the individual author(s) and contributor(s) and not of MDPI and/or the editor(s). MDPI and/or the editor(s) disclaim responsibility for any injury to people or property resulting from any ideas, methods, instructions or products referred to in the content.